Doubly Selective Underwater Acoustic Channel Model for a Moving Transmitter/Receiver

Chunshan Liu, Yuriy V. Zakharov, *Senior Member, IEEE*, and Teyan Chen

***Abstract*—We propose a new method of modeling the signal transmission in underwater acoustic communications when the transmitter and receiver are moving. The motion-induced channel time variations can be modeled by sampling the transmitter/receiver trajectory at the signal sampling rate and calculating, for each position, the channel impulse response from the acoustic-field computation. This approach, however, would result in high complexity. To reduce the complexity, the channel impulse response is calculated for fewer (*waymark*) positions and then interpolated by local splines to recover it at the signal sampling rate. To allow higher distances between waymarks and, thus, further reduction in the complexity, the multipath delays are appropriately adjusted before the interpolation. Because, for every time instant, this method only requires local information from the trajectory, the impulse response can recursively be computed, and therefore, the signal transmission can be modeled for arbitrarily long trajectories. An approach for setting the waymark sampling interval is suggested and investigated. The proposed method is verified by comparing the simulated data with data from real ocean experiments. For a low-frequency shallow-water experiment with a moving source that transmits a tone set, we show that the Doppler spectrum of the received tones is similar in the simulation and experiment. For a higher frequency deep-water experiment with a fast-moving source that transmits orthogonal frequency-division multiplexing (OFDM) communication signals, we investigate the detection performance of a receiver and show that it is similar in the simulation and experiment.**

***Index Terms*—B-spline, channel modeling, channel simulator, Doppler spread, local splines, orthogonal frequency-division multiplexing (OFDM), underwater acoustic communications.**

NOMENCLATURE

$(\cdot)^T$	Matrix transpose.
$\mathbf{C}^{(m)}$	mth column of a matrix $\mathbf{C}$.
m	Index for waymarks.
n	Index for signal samples.
i	Index for taps of the channel impulse response.
k	Index for frequencies.
$\Re\{\cdot\}$	Real part.

Manuscript received May 4, 2011; revised September 15, 2011 and December 14, 2011; accepted January 18, 2012. Date of publication February 7, 2012; date of current version March 21, 2012. This paper was presented in part at the Fourth Underwater Acoustic Measurements: Technologies, and Results Conference, Kos, Greece, June 20–24, 2011. The review of this paper was coordinated by Prof. T. Kuerner.

The authors are with the Department of Electronics, University of York, YO10 5DD York, U.K. (e-mail: cl563@ohm.york.ac.uk; yz1@ohm.york.ac.uk; tc512@ohm.york.ac.uk).

Color versions of one or more of the figures in this paper are available online at http://ieeexplore.ieee.org.

Digital Object Identifier 10.1109/TVT.2012.2187226

I. INTRODUCTION

The performance of underwater acoustic communication systems is heavily dependent on the propagation environment. The underwater channel is considered one of the most difficult channels for communications [1]. For assessing the communications performance, sea experiments are required. Although sea experiments are ultimate means of assessing the performance, they are difficult to conduct and are very expensive. In some situations, instead, the simulation of the propagation channel can be used. The simulation also has other advantages compared to experiments. For example, due to the highly dynamic time and space variability of the underwater environment, it is difficult to guarantee similar experimental conditions when comparing different systems. It is also difficult to provide reliable monitoring of the environment and thus give valuable interpretation of experimental results. Furthermore, ocean experiments with multiple users (such as in underwater communications networks) are even more complicated. On the other hand, computer simulation can provide exactly the same propagation conditions when investigating different systems, precise monitoring of the environment, and modeling communication networks with multiple users. However, this case is possible only if the simulator can provide results similar to the results observed in sea experiments. Thus, an efficient approach for simulating underwater acoustic signal transmission is highly desirable [2]–[4].

Two important phenomena that affect the performance of underwater acoustic communications are multipath propagation and the Doppler effect [2], [3], [5], [6]. Thus, the underwater acoustic channel is doubly selective. Although, time-varying multipath channel models are widely used to analyze radio communication systems (see [7]–[9] and the references therein), they are not directly applicable to underwater acoustic communications [2], [10]. For radio communications, Jakes' model combined with a set of standard power delay profiles with fixed multipath delays is often considered useful for studying the system performance [11]. The important feature of the underwater acoustic channel is the fast variation of multipath delays due to a low speed of sound. As a result, the signal distortion that is caused by the Doppler effect in the underwater channel includes the time compression/dilation that is different for different multipath components (see [2], [6], [12]–[15], and the references therein). Another important consideration is that a particular sea area can provide specific propagation conditions that should be taken into account when studying underwater acoustic systems. To account for the phenomena in the channel

model, the time-varying channel impulse response needs to be computed for a specific sea area.

Time variations of the underwater acoustic channel are caused by several factors such as the transmitter/receiver motion [2], internal waves [16], surface waves [17], [18], and others. In this paper, we focus on time variations that are caused by the transmitter/receiver motion. However, other phenomena can also be incorporated into the proposed model.

Extensive effort has been devoted in the literature to modeling underwater acoustic signal transmission. A channel simulator in [19] is based on a static channel impulse response computed by solving the underwater acoustic wave propagation equation using the normal-mode method [20] or the ray-tracing method [21]. This approach, however, does not account for transmitter/receiver movement; thus, the Doppler effect is not considered. A simulator in [22] models fluctuations of the amplitude and phase of eigenpaths (with fixed delays) as random processes. However, it is unclear how statistics of the random processes should be defined, depending on a particular sea area. In addition, this model does not consider the delay variations and, therefore, cannot accurately model the Doppler effect. The simulator proposed in [10] incorporates the Doppler effect by introducing different frequency shifts in different eigenpaths; it then uses some statistical model for varying the multipath amplitudes. However, it does not model the time-varying multipath delays, and it is unclear how statistics of the amplitude variations should be defined.

One general approach for the simulation of signal transmission is to compute the channel impulse response for transmitter/receiver positions that correspond to all sampling instants of the signal. In [18], a method was developed to generate the channel impulse response by interpolating eigenpaths that were precomputed at a regular space grid in the area surrounding the transmitter/receiver trajectory. However, for complicated and/or long-time movements, where the numbers of grid points and of signal samples are large, the complexity of this approach is high.

In this paper, we propose a different approach for modeling the underwater signal transmission that has a relatively low complexity and can be used together with different field computation methods. In this approach, the trajectory is sampled at a low rate (much lower than the signal sampling rate). At every trajectory-sampling instant, a *waymark* impulse response is computed using a field computation method, e.g., the normal-mode or ray-tracing method. Using the waymark impulse responses and adjusting the multipath delays, the time-varying impulse response is recovered using local splines. The signals are then modeled by compensating for the adjusted delays and convolving the transmitted signal with the time-varying impulse response. The proposed approach employs recursive (in time) computations, thus allowing modeling the signal transmission for arbitrary long trajectories.

This paper is organized as follows. In Section II, the proposed approach is described. In Section III, it is applied to model signals in a shallow-water experiment. In Section IV, the proposed approach is used for modeling signals in a deep-water experiment. Finally, Section V draws the conclusions.

II. Underwater Acoustic Channel Simulator

In a time-varying channel, the noise-free signal at a receiver is described as a convolution, i.e.,

$$y(t) = \int_{-\infty}^{\infty} h(t,\tau)s(t-\tau)\,d\tau, \quad t \in [0, T_s] \tag{1}$$

of the channel impulse response $h(t,\tau)$ and the source signal $s(t)$, where T_s is the signal duration. This description of linear time-variant systems is the most general. In underwater acoustic communications, different variants of the description are used. For example, for a channel with discrete multipath components, we can use the model [11], [13], [23]

$$h(t,\tau) = \sum_{p=1}^{L} A_p(t)\delta\left(\tau - \tau_p(t)\right) \tag{2}$$

where $A_p(t)$ and $\tau_p(t)$ are the time-varying amplitudes and delays of L multipath components, and $\delta(t)$ is the Dirac delta function. If $\tau_p(t) = \tau_p - at$, we arrive at a channel model that introduces compression or dilation with a compression factor a to the received signal; this model was adopted in [13] to describe nonuniform Doppler shifts of subcarriers in an orthogonal frequency-division multiplexing (OFDM) system. If $\tau_p(t) = \tau_p - a_p t$, we obtain a model with different compression factors a_p for different multipath components as used in [23] to describe channel distortions that are introduced in OFDM signals. More complicated dependencies of delays $\tau_p(t)$ on time t allow representing time-varying compression of signals. To describe macropaths and micropaths, as well as the individual Doppler compression for different macropaths, the following underwater acoustic channel model is used [24]–[26]:

$$y(t) = \sum_{pa=a1}^{L} \int_{-\infty}^{\infty} s(\eta_p t - \tau)h_p(\tau - \tau_p)\,d\tau \tag{3}$$

where $\eta_p = 1 + a_p$ and $h_p(\tau)$ are impulse responses that describe different micropath structures for different discrete multipaths (macropaths). This model is equivalent to (1), with

$$h(t,\tau) = \sum_{p=1}^{L} h_p\left(\tau - \tau_p(t)\right) \tag{4}$$

and $\tau_p(t) = \tau_p - a_p t$. Note that the model (4) can easily incorporate the frequency-dependent absorption, as opposed to the model (2).

In discrete-time form, the received signal is given by

$$y(nT) = \sum_{i=0}^{I-1} h(nT, iT)s(nT - iT), \quad n = 0, \ldots, N-1 \tag{5}$$

where T is the signal sampling interval, I is the number of channel taps, and $N = T_s/T$. To model the time-varying channel, the impulse response $h(t,\tau)$ should be known for every sampling instant $t = nT$.

Generating the impulse response for a particular point at the trajectory is based on the acoustic-field computation, which is typically of high complexity. Therefore, generating $h(nT, \tau)$ for all n would make the simulation of long-time transmission (i.e., for high N) complicated. In this section, one method of modeling underwater acoustic signal transmission that allows reduction in the complexity is proposed. For clarity, we will concentrate on scenarios where the receiver is static and the transmitter is moving.

A. Generating the Channel Frequency Response From Acoustic-Field Computation

Different source/receiver positions will result in different propagation channels. The motion-induced channel time variations can be modeled by generating the channel impulse response for the trajectory points that correspond to signal samples. This approach can be done by defining the trajectory by the pair $[r(t), z(t)]$, where $r(t)$ is the horizontal distance between the transmitter and the receiver, and $z(t)$ is the transmitter depth at instant t, mapping the sampling instants $t = nT$ to positions $[r(nT), z(nT)]$ and finding the channel frequency response from the acoustic-field computation for a set of frequencies of interest. The channel impulse response can then be obtained from the channel frequency response by the inverse Fourier transform.

At a frequency ω_k, the channel frequency response $p(nT, \omega_k)$ can be computed by solving the wave equation that governs the propagation of underwater acoustic waves. The acoustic wave equation is defined by a set of environmental parameters such as the water density ρ, the sound speed $c(z)$ at depth z, the source depth z_s, the receiver depth z, and the horizontal distance to the source r [20]. With the knowledge of the environmental parameters, different methods can be adopted for computing the acoustic field; the most popular approaches are the normal-mode [20] and the ray-tracing [21] methods.

In the normal-mode method, assuming that the environment is range independent, the frequency response at a frequency ω_k is calculated as [20]

$$p(nT, \omega_k) = \sum_{q=1}^{Q(\omega_k)} R_q\left(\omega_k, r(nT)\right) Z_q\left(\omega_k, z(nT)\right) \quad (6)$$

where $Z_q(\omega_k, z)$ are the normal modes, and $R_q(\omega_k, r)$ are expansion coefficients. The main drawback of this method is that the normal modes should be repeated for each frequency required; this approach is computationally expensive. In addition, the number of normal modes $Q(\omega_k)$ to be taken into account increases at higher frequencies [20].

The ray-tracing method [21] is based on computing L eigenpaths, starting from the source and hitting the receiver. The propagation delays $\tau_{nl}(\omega_k)$ and attenuations $a_{nl}(\omega_k)$ computed for the lth eigenpath at the position $[r(nT), z(nT)]$ are then used to compute the channel frequency response as

$$p(nT, \omega_k) = \sum_{l=1}^{L} a_{nl}(\omega_k) e^{-j\omega_k \tau_{nl}(\omega_k)}. \quad (7)$$

Compared with the normal-mode method, the ray-tracing method is more efficient at dealing with high frequencies [20].

Because the channel frequency response should be calculated for N points of the trajectory, assuming K frequencies of interest ω_k, the field computation (e.g., the normal-mode or ray-tracing method) should be repeated KN times. For example, to model the deep-water signal transmission for the experiment in Section IV, with $N \approx 10^7$ and $K \approx 10^3$, about 10^{10} field computations would then be required. This approach will result in high complexity. The complexity can be reduced by assuming that the multipath arrivals can approximately be treated as frequency independent [18]. However, this step still requires $N \approx 10^7$ field computations. In the following steps, we aim at reducing this complexity.

B. Generating the Channel Impulse Response

The (real-valued) channel impulse response for the position $[r(nT), z(nT)]$ can be computed as

$$h(nT, iT) = \Re\left\{ \frac{2}{K} \sum_{k=0}^{K-1} p(nT, \omega_k) e^{j\omega_k iT} \right\} \quad (8)$$

where $\omega_k = (\omega^- + k\delta\omega) \in [\omega^-, \omega^+]$, $\omega^- > 0$ and $\omega^+ > 0$, $\omega^+ = \omega^- + (K-1)\delta\omega$, $j = \sqrt{-1}$, $K = (\omega^+ - \omega^-)/(\delta\omega) + 1$, and $i = 0, \ldots, I-1$. In general, the frequency sampling interval $\delta\omega$ is determined from the maximum propagation delay $\tau_{\max}$ as

$$\delta\omega \leq \frac{\pi}{\tau_{\max}}. \quad (9)$$

In underwater acoustic channels, if the distance between the transmitter and the receiver is high, due to the low speed of sound, $\tau_{\max}$ will be high, and with the small $\delta\omega$, the number K of frequencies at which the acoustic field should be computed will also be high; this condition will result in high complexity of computing the frequency response.

Because the impulse response $h(nT, \tau)$ is only nonzero for a relatively short delay interval $\tau \in [\tau_{\min}, \tau_{\max}]$ and $\tau_{\min}$ is usually close to $\tau_{\max}$, i.e., $(\tau_{\max} - \tau_{\min})/\tau_{\max} \ll 1$, we can write

$$\tilde{h}(nT, iT) = \Re\left\{ \frac{2}{K} \sum_{k=0}^{K-1} p(nT, \omega_k) e^{j\omega_k (iT + \tau_{\min})} \right\} \quad (10)$$

where $\tilde{h}(nT, iT) = h(nT, iT + \tau_{\min})$. Thus, we can replace the filtering of a signal with the impulse response $h(nT, iT)$ by a filtering with the impulse response $\tilde{h}(nT, iT)$ and an extra signal delay $\tau_{\min}$. Thus, the number of channel taps I can be reduced from $I \sim \tau_{\max}/T$ to $I \sim (\tau_{\max} - \tau_{\min})/T$. Moreover, the frequency step $\delta\omega$ is then calculated as

$$\delta\omega \leq \frac{\pi}{\tau_{\max} - \tau_{\min}}. \quad (11)$$

Compared with (9), (11) allows higher $\delta\omega$ and smaller K, thus resulting in lower complexity of computing the frequency response, particularly when the distance is long such that $\tau_{\min}$ is close to $\tau_{\max}$, i.e., $(\tau_{\max} - \tau_{\min})/\tau_{\max} \ll 1$.

C. Waymarks and Local-Spline Interpolation

The variation of the channel impulse response from one signal sample to another can often be considered slow. Therefore, the computation of the impulse response for every signal sample will be redundant, and the trajectory sampling interval T_w can be made much higher than the signal sampling interval T, i.e., $T_w \gg T$. Then, an interpolation procedure can be used for recovering the time-varying impulse response for all signal sampling instants. In particular, we obtain $(M+1)$ waymark impulse responses $h_m(iT) = h(mT_w, iT)$, where $i = 0, \ldots, I-1$, $0 \le mT_w \le T_s$, $m = 0, \ldots, M$, and $T_w = T_s/M$.

To approximate time-variant channels, basis expansion models (BEMs) are widely used. The most often used BEMs are the Karhunen–Loeve (KL) functions [27], [28], discrete prolate spheroidal (DPS) functions [29], [30], complex exponentials (CEs) [29], [31], [32], and B-splines [33], [34]. To describe channel time variations $h(t, iT)$ at a specific delay (tap) iT using a BEM, we have the following approximation of $h(t, iT)$:

$$\hat{h}(t, iT) = \sum_{m=0}^{N_{b-1}} c_{i,m} b_m(t) \tag{12}$$

where $b_m(t)$ are the N_b basis functions, and $c_{i,m}$ are expansion coefficients for the ith channel tap. The use of the KL functions requires statistics of the path amplitude fluctuations to be known; however, we use a deterministic channel model. The KL, DPS, CE, and many other basis functions should be defined over the entire interval $[0, T_s]$. However, this approach would require the following three steps: 1) computing and keeping in memory all waymark impulse responses over $[0, T_s]$ before expansion coefficients can be computed, 2) computing all expansion coefficients at once, and 3) keeping in memory and using all the expansion coefficients for computing the channel impulse response at any particular signal sampling instant. With high T_s, this results in high complexity and high memory consumption.

We use local splines, which allow significant reduction in the complexity and memory requirement compared to the aforementioned basis functions. With the same number of basis functions, we can achieve similar performance as with an orthogonal basis [35], [36]. When using cubic B-splines, only four expansion coefficients and four basis functions are needed to compute the impulse response at any sampling instant. Furthermore, to compute an expansion coefficient, only a finite number (three in our case) of waymark impulse responses are needed. Thus, for the computation of the signal at the output of the channel at any instant, we only need a few waymark impulse responses. For example, for the cubic spline approximation that we are using, for any time instant, only six waymark impulse responses are required. In addition, all basis functions are time-shifted versions of a single B-spline that have a finite support ($4T_w$ for the cubic B-spline), which is usually much smaller than T_s. First, this approach significantly reduces the modeling complexity. Second, it allows a recursive computation of the output signal with reduced and fixed memory consumption, independent of the signal duration.

Cubic splines provide good tradeoff between the complexity and accuracy of approximation compared to other spline orders [37]. We use local cubic splines for our model; however, other local splines can also be used [33], [38], [39]. The expansion (12) is then converted into [37]

$$\hat{h}(t, iT) = \sum_{m=-1}^{M+1} c_{i,m} b(t - mT_w) \tag{13}$$

where we use $N_b = M + 3$, and $b(t)$ is the cubic B-spline, which is given by

$$b(t) = \begin{cases} \frac{1}{6}\left(2 - \frac{|t|}{T_w}\right)^3 - \frac{2}{3}\left(1 - \frac{|t|}{T_w}\right)^3, & 0 \le |t| < T_w \\ \frac{1}{6}\left(2 - \frac{|t|}{T_w}\right)^3, & T_w \le |t| < 2T_w \\ 0, & \text{otherwise.} \end{cases} \tag{14}$$

The expansion coefficients $c_{i,m}$ for the local splines are found as [33], [38]

$$c_{i,m} = a_{-1} h_{m-1}(iT) + a_0 h_m(iT) + a_1 h_{m+1}(iT) \tag{15}$$

where $a_1 = a_{-1} = -1/6$, and $a_0 = 4/3$.

The spline interpolation can be represented in matrix form. Let $\mathbf{h}_m = [h_m(0) \;\; h_m(T) \;\; \ldots \;\; h_m(IT - T)]^T$ and $\mathbf{c}_m = a_{-1}\mathbf{h}_{m-1} + a_0\mathbf{h}_m + a_1\mathbf{h}_{m+1}$. Then

$$\hat{\mathbf{h}}(T) = \sum_{m=-1}^{M+1} \mathbf{c}_m \mathbf{b}(t - mT_w).$$

Because the support of the cubic B-spline (14) is $4T_w$, for each time instant t, only four spline coefficients $\mathbf{c}_m$ are required. Therefore, for $t = nT \in [mT_w, mT_w + T_w]$, we have

$$\hat{\mathbf{h}}(nT) = \mathbf{C}\mathbf{b}(nT) \tag{16}$$

where $\mathbf{C} = [\mathbf{c}_{m-1} \;\; \mathbf{c}_m \;\; \mathbf{c}_{m+1} \;\; \mathbf{c}_{m+2}]$, $\mathbf{b}(nT) = [b(\xi + T_w) \; b(\xi) \; b(\xi - T_w) \; b(\xi - 2T_w)]^T$, and $\xi = nT - mT_w$.

Note that, if T_w is chosen to be a multiple of T, then the vectors $\mathbf{b}(nT)$ can be precomputed for all possible ξ within one interval T_w and stored. Thus, recomputing this vector for each signal sample is not required. It is also shown that, for each time instant nT, the spline interpolation has a recursive form with only six waymark impulse responses in the vicinity of the trajectory point $[r(nT), z(nT)]$ involved and that no other information is required. This condition is beneficial when modeling long-time signal transmission.

D. Delay Adjustment

Due to the low speed of sound, a small deviation of the transmitter/receiver position may result in significant deviation of the multipath propagation delays. With a high T_w, this condition can result in significant interpolation errors [4]. Fig. 1(a) shows two adjacent waymark impulse responses that were obtained for a single-path environment. We assume that the source moves at a constant horizontal speed of 6 m/s and that the channel delay varies in time as a linear function. Using $T_w = 125$ ms, i.e., the horizontal distance between two waymarks on the trajectory is 0.75 m, leads to an increase in the

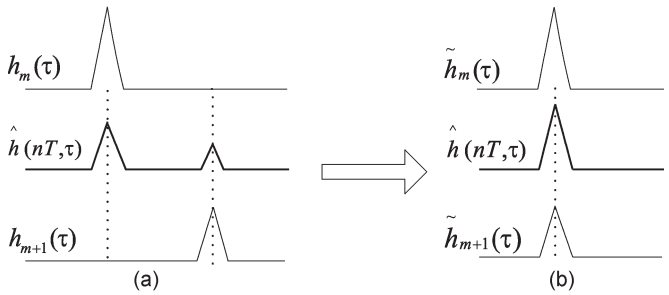

Fig. 1. Example of the interpolation of the channel impulse response. (a) Without delay adjustment. (b) With delay adjustment.

delay between two waymarks by about 0.5 ms. When modeling signal transmission at a sampling rate of 10 kHz, this delay difference is as large as five signal samples. If we apply (for simplicity) linear interpolation to obtain an impulse response at a time instant between the two waymarks, the result is a two-path impulse response $\hat{h}(nT,\tau)$ (instead of a true single-path response), as shown in Fig. 1(a). Thus, the multipath structure of the channel is destroyed.

To overcome this problem, we will try to compensate for the delay shifts between consecutive waymark impulse responses. Note that different multipath delays have different variations; therefore, in general, the precise compensation is infeasible. We can only achieve an approximate delay adjustment. This step can be done in different ways. As an example, all the waymark impulse responses can be aligned with respect to the first multipath arrival. This approach, however, can encounter problems for some scenarios due to the possibility that the first arrival can disappear at some point of the trajectory. Another problem is that the first arrival can have the Doppler effect (i.e., the delay variation rate) quite different from other multipaths. We have found the following approach for aligning the time-varying impulse response efficient in many scenarios.

A delay shift Δ between two consecutive waymarks $m-1$ and m can be found by solving the following problem:

$$\Delta = \arg\max_{\Theta} J(\Theta) \tag{17}$$

where $J(\Theta) = |\sum_{k=0}^{K-1} p_m(\omega_k) p_{m-1}^*(\omega_k) e^{j\omega_k \Theta}|^2$. This problem is equivalent to the frequency estimation problem, and it can be solved by several techniques. We have found that the dichotomous search similar to the technique in [40] is useful for this purpose. The corresponding algorithm is presented in Table I.

The algorithm searches for the best match Δ for the two waymark frequency responses $p_m(\omega_k)$ and $p_{m-1}(\omega_k)$ in an interval $[q^-\delta_{\text{init}}, q^+\delta_{\text{init}}]$, where δ_{init} is an initial step size, and q^+ and q^- are integers. The initialization $\delta_{\text{init}} = T/2$ is found to be a good choice. Assuming that the minimum (maximum) speed of the transmitter is $v_{\min}$ ($v_{\max}$), the values q^- and q^+ can be found from the inequalities

$$q^+\delta_{\text{init}} > \frac{v_{\max} T_w}{c_0}, \quad q^-\delta_{\text{init}} < \frac{v_{\min} T_w}{c_0}$$

where $c_0 = 1500$ m/s.

TABLE I
DELAY ADJUSTMENT

Input:
q^-, q^+, δ_{init}, Q, $p_{m-1}(\omega_k)$, $p_m(\omega_k)$, $k = 0, \ldots, K-1$
Initialization:
$\delta = \delta_{\text{init}}$
$q_{\max} = \arg\max_{q=q_{\text{lower}},\ldots,q_{\text{upper}}} \{J(q\delta)\}$
where $J(\Delta) = \left\lvert \sum_{k=0}^{K-1} p_m(\omega_k) p_{m-1}^*(\omega_k) e^{j\omega_k \Delta} \right\rvert^2$
$\Delta = q_{\max}\delta$
$J_1 = J(\Delta - \delta)$, $J_2 = J(\Delta)$, $J_3 = J(\Delta + \delta)$
Repeat Q times:
$\delta \leftarrow \delta/2$
if $J_3 < J_1$ then $J_3 = J_2$ and $\Delta \leftarrow \Delta - \delta$
else $J_1 = J_2$ and $\Delta \leftarrow \Delta + \delta$
$J_2 = J(\Delta)$

The algorithm runs Q iterations, in which the step size δ is halved $\delta \leftarrow \delta/2$, and the solution Δ is rectified so that the final resolution is $\delta_{\text{init}}/2^Q$. A *waymark composite delay* is then found as

$$\tau_m = \tau_{m-1} + \Delta, \quad \tau_0 = \tau_{\min}.$$

The delay-adjusted waymark impulse response, considering the composite delay, is then generated as

$$\tilde{h}_m(iT) = \Re\left\{ \frac{2}{K} \sum_{k=0}^{K-1} p_m(\omega_k) e^{j\omega_k (iT + \tau_m)} \right\}$$

i.e., $\tilde{h}_m(iT) = h_m(iT + \tau_m)$.

The delay-adjusted impulse response $\tilde{\mathbf{h}}_m = [\tilde{h}_m(0) \ \ldots \ \tilde{h}_m(IT - T)]^T$ will now replace $\mathbf{h}_m$ in the local interpolation described in Section II-C. Fig. 1(b) illustrates the benefit of the delay adjustment for the interpolation of the channel impulse response.

E. Waymark Sampling Period

We now discuss how the trajectory space sampling interval Δr and, consequently, the waymark sampling period T_w can be chosen. First, we can use the trial-and-error approach. Several values of T_w can be tried, and an interval that provides a small-enough error, e.g., the mean square error (MSE) between the interpolated and original (from the acoustic-field computation) impulse responses, as explained in Sections III and IV, can be used for the simulation.

Alternatively, the choice of Δr and T_w can be done based on the waveguide invariant theory [41], [42]. In particular, we can write

$$\left| \frac{\Delta\omega}{\Delta r} \right| = \beta \left| \frac{\omega_{\max}}{r} \right|$$

where $\Delta\omega$ is a frequency shift of a maximum $\omega_{\max}$ in the channel frequency response magnitude due to the horizontal movement of a transmitter from distance r to $r + \Delta r$, and $\beta \approx 1$ is the waveguide invariant [41]. Due to the horizontal movement, the multipath delays are varying. We want to choose the range increment Δr so that a delay variation $\Delta\tau$ satisfies the condition $\Delta\tau \ll T$. With such a choice, fluctuations of the

impulse response at fixed delays due to delay variations will be negligible.

Consider the following simplified scenario. At a distance r, let the channel have two equally strong multipath components of a unit amplitude separated by a delay τ. The magnitude of the channel frequency response is then given by $H(\omega) = 2 + 2\cos(\omega\tau)$. The maximum of $H(\omega)$ is observed at frequencies $\omega_{\max} = 2\pi k/\tau$, where $k \geq 1$ is an integer. Due to the horizontal movement from r to $r + \Delta r$, the multipath delays change; therefore, the magnitude of the frequency response is now $H_\Delta(\omega) = 2 + 2\cos(\omega(\tau + \Delta\tau))$. The maximum of $H(\omega)$ is now shifted to the frequency $\omega_{\max} + \Delta\omega = 2\pi k/(\tau + \Delta\tau)$. Based on this equation, we find that $(\Delta\omega/\omega_{\max}) = -\Delta\tau/(\tau + \Delta\tau)$, and we obtain

$$\Delta r = \frac{1}{\beta}\left|\frac{\Delta\omega}{\omega_{\max}} r\right| \approx \frac{\Delta\tau}{\tau + \Delta\tau} r.$$

We are interested in obtaining delay variations $\Delta\tau$ that are much smaller than the signal sampling interval T, i.e., Δr should be small enough to guarantee that $\Delta\tau \ll T$; thus

$$\Delta r \ll \frac{T}{\tau + \Delta\tau} r \approx \frac{T}{\tau} r.$$

For a fixed horizontal speed v_0 of the transmitter, we then arrive at the waymark sampling interval $T_w = \Delta r/v_0$. Although this scenario is simple, we found that the aforementioned relationship is useful for choosing the waymark sampling interval for experimental scenarios. To apply this relationship in other scenarios, we note that τ is the multipath delay spread of the channel. Note that this choice is based on the assumption that the impulse responses at waymark points are aligned, as explained in Section II-D. In Sections III and IV, we show how this choice relates to the MSE.

F. Generating the Channel Output Signal

To generate the channel output signal, we need the following steps for every signal sample instant nT.

1) Compute the channel impulse response (this step is done through the local spline interpolation of the waymark impulse responses $\tilde{h}_m(iT)$ as aforementioned).
2) Compute and compensate for a composite delay $\hat{\tau}(nT)$.
3) Convolve the input signal with the impulse response $\hat{\mathbf{h}}(nT)$.

To compute the composite delay, we can again use the local spline interpolation similar to (16), i.e.,

$$\hat{\tau}(nT) = \boldsymbol{\theta}^T \mathbf{b}(nT)$$

where $\boldsymbol{\theta} = [\theta_{m-1}\ \theta_m\ \theta_{m+1}\ \theta_{m+2}]^T$, and $\theta_m = a_{-1}\tau_{m-1} + a_0\tau_m + a_1\tau_{m+1}$.

Compensation for the composite delay can be done as follows. A signal vector $\tilde{\mathbf{s}}(nT)$ of length I is computed with the elements that were obtained through the interpolation of the signal $s(t)$ at instants $t = nT - iT - \hat{\tau}(nT)$, $i = 0, \ldots, I-1$. The interpolation can be done using the local splines or any other method. The convolution then takes the form

$$y(nT) = \tilde{\mathbf{s}}^T(nT)\hat{\mathbf{h}}(nT).$$

TABLE II
CHANNEL SIMULATOR

Input:
$c(z)$, ρ, $[r(t), z(t)]$, $[\omega^-, \omega^+]$, T, $\tau_{\min}$, $\tau_{\max}$, $\delta\omega$, T_w, I, N

Initialization:
Repeat for $m = -2, \ldots, 3$**:**
Compute the frequency response $p_m(\omega_k)$, $k = 0, \ldots, K-1$, for position $[r(mT_w), z(mT_w)]$ using acoustic field computation
Find the composite delay τ_m using a delay adjustment algorithm
Compute $\tilde{p}_m(\omega_k) = p_m(\omega_k)\exp(j\omega_k\tau_m)$
Compute the *waymark* impulse response $\tilde{\mathbf{h}}_m$ with elements:
$\tilde{h}_m(iT) = \Re\left\{\frac{2}{K}\sum_{k=0}^{K-1}\tilde{p}_m(\omega_k)\exp(j\omega_k iT)\right\}$, $i = 0, \ldots, I-1$
Repeat for $m = -1, \ldots, 2$**:**
Compute spline coefficients for the impulse response:
$\mathbf{c}_m = a_{-1}\tilde{\mathbf{h}}_{m-1} + a_0\tilde{\mathbf{h}}_m + a_1\tilde{\mathbf{h}}_{m+1}$
Compute a spline coefficient for the composite delay:
$\theta_m = a_{-1}\tau_{m-1} + a_0\tau_m + a_1\tau_{m+1}$
Form an $I \times 4$ matrix: $\mathbf{C} = [\mathbf{c}_{-1}\ \mathbf{c}_0\ \mathbf{c}_1\ \mathbf{c}_2]$
Form an 4×1 vector: $\boldsymbol{\theta} = [\theta_{-1}\ \theta_0\ \theta_1\ \theta_2]^T$
Set $T_h = T_w$

Repeat for $n = 0 : N-1$**:**
if $nT > T_h$
$m = m + 1$, $T_h = T_h + T_w$
Compute the frequency response $p_m(\omega_k)$, $k = 0, \ldots, K-1$, for position $[r(mT_w), z(mT_w)]$
Find the composite delay τ_m
Compute $\tilde{p}_m(\omega_k) = p_m(\omega_k)\exp(j\omega_k\tau_m)$
Compute the *waymark* impulse response $\tilde{\mathbf{h}}_m$
Compute spline coefficients for the impulse response:
$\mathbf{c} = a_{-1}\tilde{\mathbf{h}}_{m-2} + a_0\tilde{\mathbf{h}}_{m-1} + a_1\tilde{\mathbf{h}}_m$
Update $\mathbf{C}$: $\mathbf{C}^{(u)} = \mathbf{C}^{(u+1)}$, $u = 1, 2, 3$, and $\mathbf{C}^{(4)} = \mathbf{c}$
Compute spline coefficient for the composite delay:
$\theta_m = a_{-1}\tau_{m-2} + a_0\tau_{m-1} + a_1\tau_m$
Update $\boldsymbol{\theta}$: $\boldsymbol{\theta} = [\theta_{m-3}\ \theta_{m-2}\ \theta_{m-1}\ \theta_m]^T$
end if
$\xi = nT - T_h + T_w$
$\mathbf{b}(nT) = [b(\xi + T_w)\ b(\xi)\ b(\xi - T_w)\ b(\xi - 2T_w)]^T$
Spline interpolation of the impulse response: $\hat{\mathbf{h}} = \mathbf{C}\mathbf{b}$
Spline interpolation of the composite delay: $\hat{\tau}(nT) = \boldsymbol{\theta}^T\mathbf{b}$
Interpolation of the signal: $\tilde{s}(iT) \leftarrow s(nT - iT - \hat{\tau}(nT))$
Convolution: $y(nT) = \sum_{i=0}^{I-1}\hat{h}(nT, iT)\tilde{s}(iT)$

The channel model is now summarized in Table II.

The proposed simulator significantly reduces the time for computing the acoustic field compared to the direct computation at the signal sampling rate f_s. For example, computing the impulse response for one space point of the deep-water experiment, as described in Section IV, using the ray-tracing program BELLHOP [43] on a personal computer (4-GB memory, Intel CPU E8500, clocked at 3 GHz) takes approximately 3 s. Thus, generating a 100-s signal at the sampling rate $f_s = 12288$ Hz would take about $3.6 \cdot 10^6$ s or 42 days. In the proposed simulator using $T_w = 0.2$ s, for a 100-s signal, approximately 500 waymarks are required. Thus, computing the waymark impulse responses takes about 25 min. Note that other computations for generating the signal, which are implemented in MATLAB, also take about 25 min. Thus, the whole computation of the 100-s signal takes about 50 min.

Fig. 2 shows the structure of the proposed simulator. The part of the simulator that deals with computations at the waymark rate $1/T_w$ (acoustic field, waymark impulse response, and composite delay computations) is separated from the part that performs the signal processing at the signal sampling rate f_s. The latter step can be implemented in real time, provided that the waymark impulse responses and composite delays have been precomputed. Finite-impulse-response (FIR)

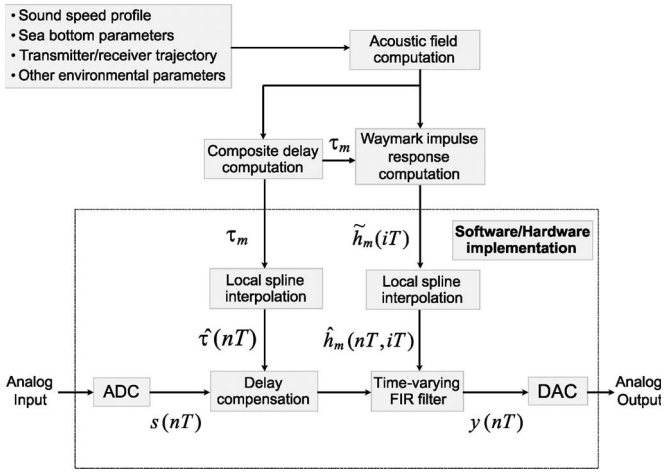

Fig. 2. Underwater acoustic channel simulator.

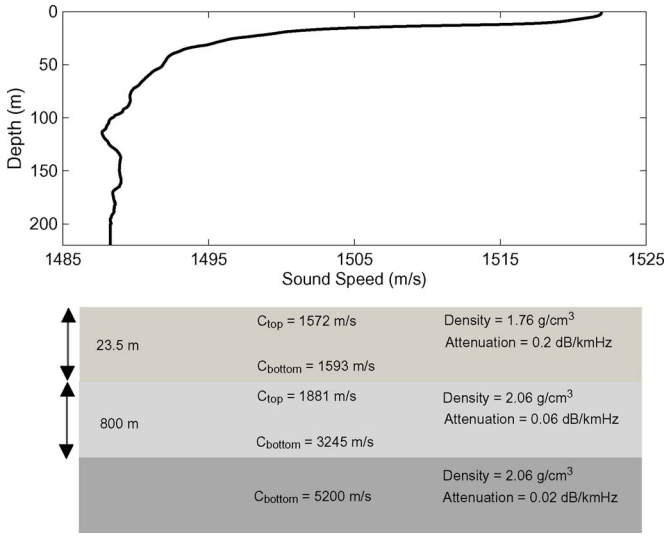

Fig. 3. SSP for the experiment SWellEx-96 (Event S5).

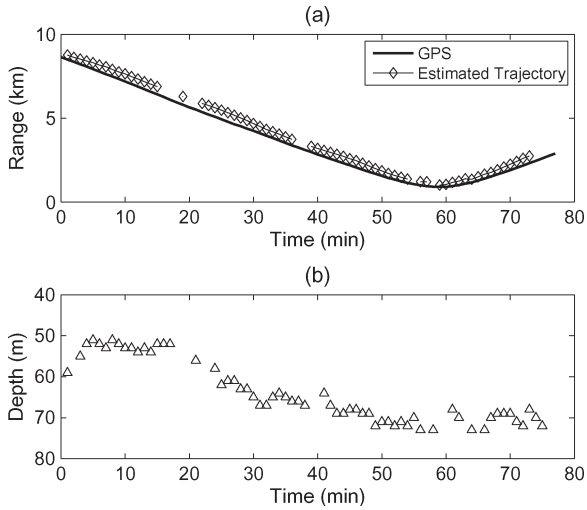

Fig. 4. Trajectory of the source in the experiment SWellEx-96 (Event S5). (a) Estimated range and range from GPS measurements. (b) Estimated depth.

filtering requires I multiply–accumulate (MAC) operations per sample. The delay compensation using the cubic local splines requires three MAC operations per sample. The local spline interpolation of the waymark impulse response requires $3I$ MAC operations per waymark interval T_w to compute the spline coefficients according to (15) and $4I$ MAC operations per sample to interpolate the impulse response at the rate f_s according to (13). Note that the B-spline (14) does not need to be computed in real time, because it can be precomputed on a uniform grid within the signal sampling interval T; for example, the precomputation with a grid step of $T/1000$ would only require $4 \cdot 10^3$ memory while introducing a negligible error in the recovered signal [33]. Similarly, local spline interpolation of the signal according to the composite delay requires four MAC operations per sample. In total, as $T_w \gg T$, the part indicated as "Software/Hardware Implementation" in Fig. 2 requires approximately $5I + 4$ MAC operations per sample or about $5If_s$ MACs/s. As the number of taps $I \approx \tau f_s$, where τ is the multipath delay spread, the number of operations has a quadratic dependence on the sampling frequency f_s. For example, for the Pacific Ocean experiment described in Section IV, with the sampling frequency $f_s = 12288$ Hz and the number of filter taps $I = 7000$, the complexity is $5 \times 12288 \times 7000 \approx 430 \cdot 10^6$ MACs/s. This approach can be implemented in real time using modern digital signal processing and/or field-programmable gate-array design platforms. Note that the complexity of this part of the simulator is almost independent of the waymark interval T_w, i.e., the speed of the source. However, the complexity of the part that deals with computations at the waymark rate T_w will proportionally be increased.

III. Shallow-Water Experiment

In this section, we apply the proposed approach to model signal transmission in an environment that corresponds to the shallow-water experiment SWellEx-96 (Event S5) [44]. We show that the numerical simulation results match well with the experimental results.

During the experiment, a ship that tows a deep source at a supposed depth of 54 m moved from a distance of 9 km toward and beyond a vertical line array (VLA) at a speed of 2.5 m/s. Our analysis is based on data that were collected on the VLA that consists of 21 hydrophones at depths between 94.125 and 212.25 m. The signal sampling rate is $f_s = 1/T = 1500$ Hz. The source simultaneously transmitted a set of 13 tones at frequencies from 49 Hz to 388 Hz. The sound speed profile (SSP) $c(z)$ based on [44], as shown in Fig. 3, is used in our simulation. In [45] and [46], we estimated the source range trajectory for this experiment. The estimate well matches with Global Positioning System (GPS) measurements, as shown in Fig. 4(a). An estimate of the depth trajectory is shown in Fig. 4(b). The estimated trajectory is used in our simulation to model the signals received at the 21 hydrophones.

To determine the waymark sampling period, we use the approach described in Section II-E as follows. For example, for the distance $r = 4.5$ km, the multipath delay spread found from the field computation is approximately $\tau = 0.3$ s. We need to choose the range sampling interval Δr so that $\Delta r \ll (T/\tau)r$. As $T = 1/1500$ s, we have $\Delta r \ll 10$ m. With the speed of

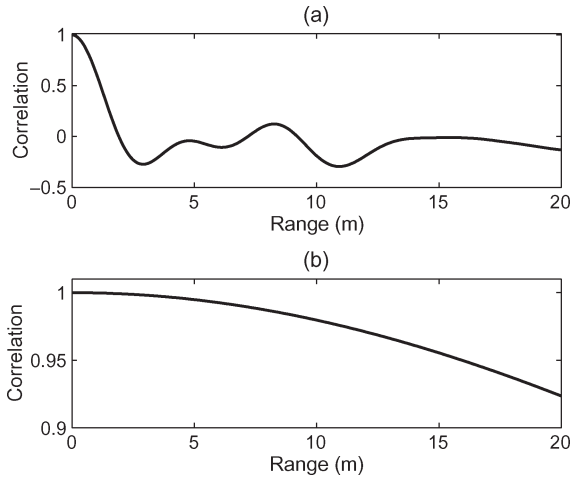

Fig. 5. Correlation of impulse response versus distance for the experiment SWellEx-96. (a) Without delay adjustment. (b) With delay adjustment.

the transmitter 2.5 m/s, we obtain that the waymark sampling interval should satisfy $T_w \ll 4$ s; in our simulation, we use $T_w = 0.5$ s.

According to Fig. 4(a), the maximum distance between the transmitter and the VLA is about 9 km, which results in a 6-s propagation time. Without the delay adjustment, the frequency step $\delta\omega$ for computing the acoustic field should be set to a value $\delta\omega/(2\pi) < 0.08$ Hz. With the delay adjustment, because the maximum multipath delay spread is 0.3 s, the frequency step can be increased so that $\delta\omega/(2\pi) < 1.5$ Hz. In our simulation, the channel frequency response is computed with a frequency step $\delta\omega/(2\pi) = 1$ Hz in a frequency interval of [40, 410] Hz. The normal-mode program KRAKEN [20] is used for the field computation.

First, the effectiveness of the delay adjustment is examined. We compute the cross correlation between impulse responses found from the field computation at different positions. The correlation as a function of delay α between two positions is calculated as

$$\nu(\alpha) = \frac{\mathbf{h}^T(t_0)\mathbf{h}(t_0+\alpha)}{\sqrt{\mathbf{h}^T(t_0)\mathbf{h}(t_0)}\sqrt{\mathbf{h}^T(t_0+\alpha)\mathbf{h}(t_0+\alpha)}} \tag{18}$$

where $\mathbf{h}(t_0)$ is the channel impulse response at a distance $r(t_0) \in [4, 5]$ km. Fig. 5 shows the correlation that was averaged over the range interval of [4, 5] km versus the distance that corresponds to α with and without the delay adjustment. Without the delay adjustment, the correlation rapidly decays as the distance increases; for $T_w = 0.5$ s (i.e., for a distance of 1.25 m), the correlation is as low as $\nu = 0.45$. After the delay adjustment, the correlation is increased to $\nu = 0.9997$. Fig. 6 shows the MSE between the impulse response that was obtained through spline approximation and the original (from the field computation) channel impulse response in the range interval of [4, 5] km. It is shown that the MSE is below -68 dB, which shows that, here, the spline interpolation is very accurate.

Fig. 7 compares the Doppler spread of the tones obtained from the experimental and simulated received signals. The Doppler spectra are obtained by averaging periodograms of the received tones over 100-s-long snapshots and over the

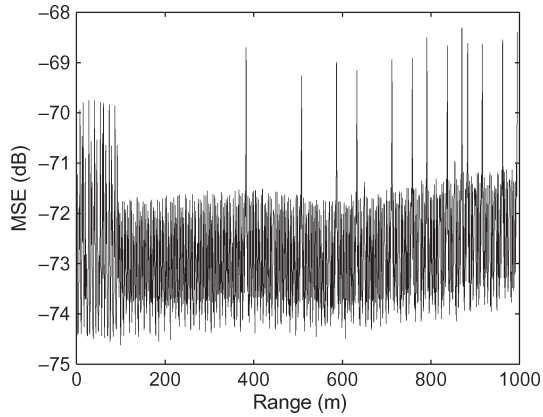

Fig. 6. MSE between the approximated and original channel impulse responses for the experiment SWellEx-96.

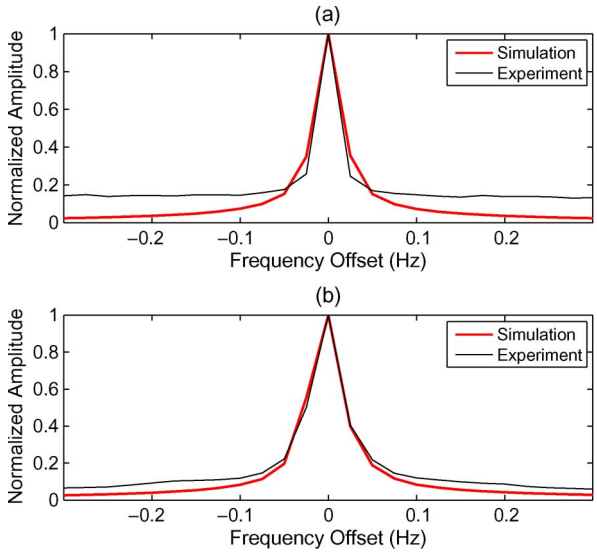

Fig. 7. Doppler spread of two tones (of frequencies f_c) obtained from the experimental and simulated signals.

21 receiver hydrophones. The frequency shifts of the tones due to the constant speed of the ship and the geometry of the experiment are removed, as described in [45] and [46]. It is shown that the Doppler spread of the modeled signals match well with the Doppler spread obtained from the experimental data. The mismatch in the floor level is due to the noise present in the experimental data and not added into the simulated signals.

IV. Deep-Water Experiment

In this section, we verify the proposed channel model on data that were obtained from a deep-water experiment in the Pacific Ocean [24]. During the experiment, an acoustic source was towed by a ship that moves toward the receiver at a supposed speed of 6 m/s and a depth of 200 m. An omnidirectional hydrophone that was positioned at a nominal depth of 400 m was used to record the received signal. The distance between the transmitter and the receiver varied from 42 km to 40 km. In the vertical plane, the transducer beampattern is approximated as having a 0-dB gain for grazing angles $|\alpha| \leq 15^\circ$ and -10 dB

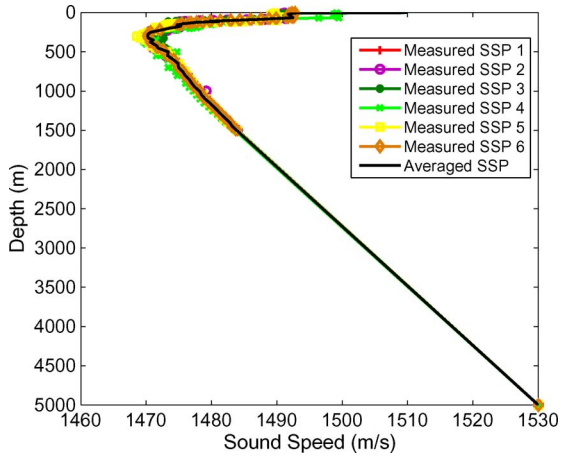

Fig. 8. SSPs $c(z)$ for the Pacific Ocean experiment.

for $15^\circ < |\alpha| < 25^\circ$. SSPs that were measured in the experiment are shown in Fig. 8. The SSP that was averaged over the measured SSPs is used in the simulation. The ray-tracing program BELLHOP [43] is used to generate eigenpaths.

In the experiment, 340 coded OFDM symbols were transmitted. One OFDM symbol is given by [24], [47]

$$s(t) = \sum_{k=0}^{N_{\rm sc}-1} \cos\left[2\pi f_k + \phi(k)\right] \tag{19}$$

where the number of subcarriers $N_{\rm sc} = 1024$, $f_k = f_c - F/2 + k/T_s$, $f_c = 3072$ Hz, the frequency bandwidth of the signal is $F = N_{\rm sc}/T_{\rm OFDM} = 1024$ Hz, and $T_{\rm OFDM} = 1$ s is the OFDM symbol duration. The phase modulation $\phi(k)$ of the subcarriers is given by

$$\sqrt{2}e^{j\phi(k)} = M_2(k) + jM_1(k) \tag{20}$$

where $M_2(k)$ is a coded bit that was transmitted at the kth subcarrier, and $M_1(k)$ is a pilot bit. The sequences $M_1(k)$ and $M_2(k)$ are binary with values $\pm$ 1. The sequence $M_2(k)$ is a rate 1/2 convolutional code generated by polynomials [247, 371] in octal [48]. The OFDM symbols are transmitted one by one without any guard interval. Thus, the information data rate in the experiment is about 500 b/s or, equivalently, ≈ 0.5 b/s/Hz.

The receiver is briefly described as follows.

First, a time-varying Doppler compression factor is estimated with a time step $T_{\rm est} \le T_{\rm OFDM}$. This is done by computing the cross-ambiguity function between the received and the pilot signals on a 2-D grid of delay and compression factor and finding the maximum on the 2-D grid [6], [24]. The compression factor estimate is further rectified by using parabolic interpolation as described in [49]. The compression factor estimates are linearly interpolated to the signal sampling rate and used to compensate for the time-varying Doppler effect by resampling the signal with the time-varying compression factor. The signal is then transformed into a complex-envelope signal within the frequency range $[-512, +512]$ Hz.

Second, linear time-domain FIR equalization with equalizer coefficients that were derived from channel estimates is applied to the complex-envelope signal. The main purpose of the equalizer is to reduce the multipath delay spread. The channel estimation is based on computing cross correlation between the pilot and complex-envelope signals and is performed with the same time step $T_{\rm est}$ as the estimation of the Doppler compression factor. The equalized signal is then transformed into the frequency domain using the fast Fourier transform.

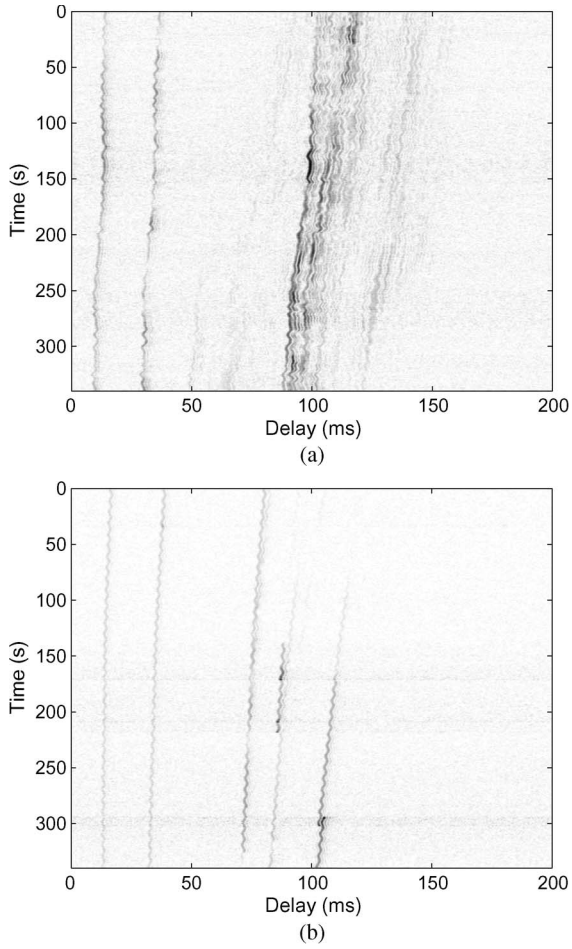

Fig. 9. Estimates of the channel impulse response. (a) From experimental data. (b) From simulated data for the sinusoid movement.

Finally, $N_{\rm turbo}$ turbo iterations ($N_{\rm turbo} = 3$ in our case) are repeated, each performing frequency-domain channel estimation, equalization, and soft-decision Viterbi decoding [48]. The channel estimation is based on the BEM with CEs. For the channel estimation, the pilot and tentative estimates of information symbols (zeros at the first turbo iteration) produced by the Viterbi decoder are used.

Fig. 9(a) shows the impulse response estimates that were obtained from the experimental data. Periodic fluctuations of multipath delays are shown. Analysis of the fluctuations shows that they are synchronous, i.e., all delays are simultaneously increased or decreased. This case is an indication of range fluctuations, as opposed to depth fluctuations of the source, in which case, if delays of multipaths that arrive at the receiver with positive grating angles increased, delays of multipaths that arrive at negative angles would decrease, and *vice versa*. In the case of depth fluctuations, we would see, in Fig. 9(a), opposite delay fluctuations for some multipath components. The range fluctuations are caused by the towing of the transducer by

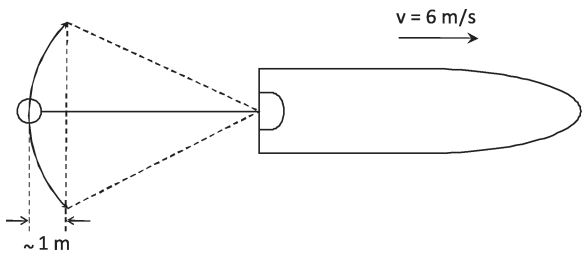

Fig. 10. Tether angle sweeping when towing the transducer.

the surface ship. This can be explained by the drawing in Fig. 10. When towing the transducer, due to the impact of the surface waves on the ship, the tether was randomly sweeping in angle, which resulted in the range fluctuations with an average amplitude of 1 m. The spectrum of the fluctuations matches well with the surface waves with an average period of about 10 s.

In the simulation, to match the experimental data, the source is modeled as moving at a constant depth with a time-varying speed (with range fluctuations), i.e.,

$$r(t) = r_o - v_o t + r_{\text{fluct}}(t) \tag{21}$$

where $r_0 = 42.16$ km, and $v_0 = 6$ m/s. In the first part of the simulation, we use a simplified "*sinusoidal movement*," i.e., $r_{\text{fluct}}(t) = \mu \sin(2\pi t/T)$, with $\mu = 1$ m. In the second part of the simulation, we use $r_{\text{fluct}}(t)$, which is derived from the experimental data.

To choose the waymark sampling interval, we apply the approach described in Section II-E. The range step Δr should be chosen to satisfy $\Delta r \ll (T/\tau)r$. In the experiment, we have $r \approx 40$ km, $T = 6.9\ 10^{-5}$ s (the signal sampling rate is $4 \cdot 3072 = 12288$ Hz), and the multipath delay spread $\tau < 0.5$ s (in addition to multipaths shown in Fig. 9(a), there are weak multipaths with delays close to 0.5 s). Thus, we obtain $\Delta r \ll 5.5$ m. With the 6-m/s speed of the transmitter, we obtain that the waymark sampling interval should satisfy $T_w \ll 0.9$ s. We consider the following two cases: 1) $T_w = 0.2$ s and 2) $T_w = 0.1$ s. The frequency step for computing the channel frequency response is set to $\delta\omega/(2\pi) = 1$ Hz.

Fig. 11 shows the MSE between the impulse response that was obtained from the acoustic-field computation and the result of the spline interpolation for the first 450 m of the trajectory. For $T_w = 0.2$ s, the MSE is close to -30 dB; however, at a distance of 280 m, the MSE increases to a level of -16 dB. The MSE peak is caused by the change in the multipath structure; in particular, at this position, some multipath components disappear. When reducing the waymark sampling interval to $T_w = 0.1$ s, the MSE peak is reduced to the level -24 dB.

We now model the signal transmission for the sinusoidal movement and estimate the time-varying impulse response from the simulated signal; the impulse response is shown in Fig. 9(b). Comparing Fig. 9(a) and (b), it is shown that the proposed simulator accurately describes the effect that was caused by fluctuations of the source movement.

We now model the source movement with $r_{\text{fluct}}(t)$, which was derived from the experimental data. In particular, the time-varying speed is computed using the time-varying Doppler

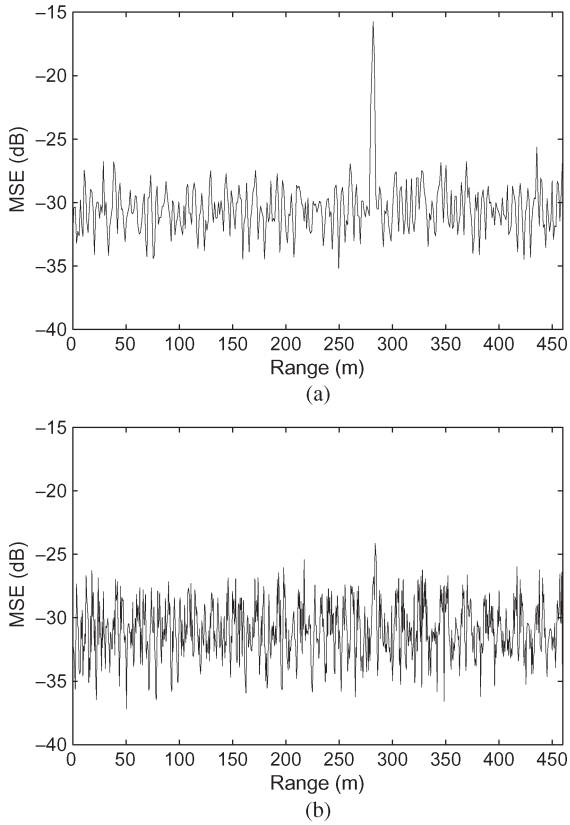

Fig. 11. MSE between the impulse responses obtained from the acoustic field computation and the local spline interpolation. (a) $T_w = 0.2$ s. (b) $T_w = 0.1$ s.

compression factor estimated from the experimental data. Fig. 12(a) shows the compression factor variations for the strongest multipath component estimated from the experimental and simulated signals. A constant compression factor due to the constant speed v_0 is removed to emphasize the fluctuations. Fig. 12(b) shows the spectrum of the fluctuations. It is shown that the results obtained in the simulation match very well with the experiment.

Next, the bit error rate (BER) and MSE performance of the receiver is investigated. In Fig. 13, the BER is shown as a function of the estimation interval T_{est}. The average signal-to-noise ratio (SNR) in the simulated signals is set to 25 dB by adding white noise, which is the same SNR as measured in the experimental data. In addition to the two scenarios where the trajectory has range fluctuations ($r_{\text{fluct}}(t) \neq 0$), we have also simulated data for the scenario with no range fluctuations ($r_{\text{fluct}}(t) = 0$), i.e., when the source moves with a constant speed of 6 m/s. By comparing the BER performance of the receiver in the three simulation scenarios and in the experiment, we have the following conclusions. The simulation results for the sinusoidal and real movements that take into account the range fluctuations both match well with the experimental data. However, the simulation results for the scenario with no range fluctuations show a lower BER (see Figs. 13 and 14 for MSE). This result is well supported by the Doppler spectrum for this scenario in Fig. 15, which shows slower channel variations compared to the variations in the case of range fluctuations (see Fig. 12). It is shown that the threshold interval T_{est} beyond which the BER significantly increases is now higher and that

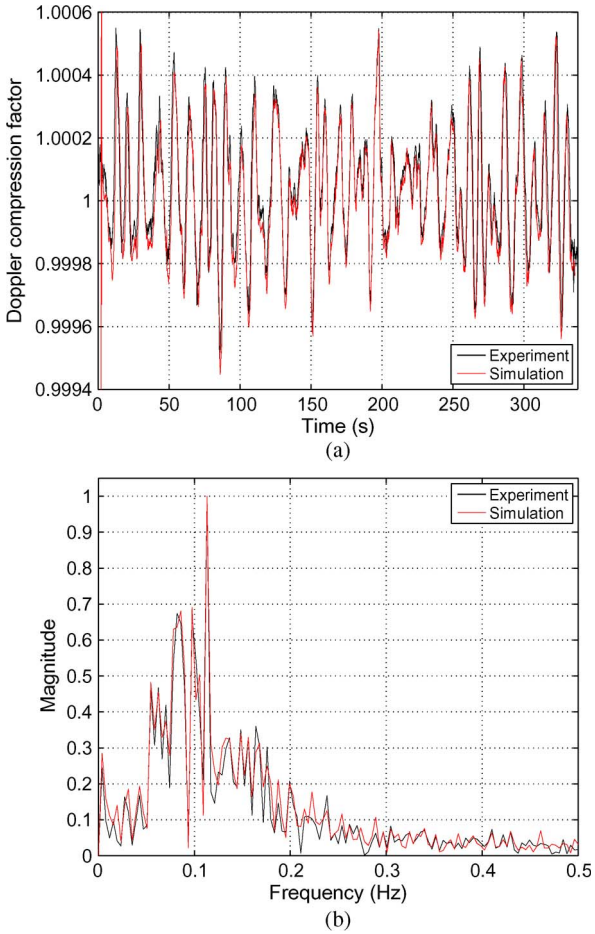

Fig. 12. Fluctuations of the compression factor in the experimental and simulated signals. (a) Fluctuations of the compression factor in time. (b) Spectrum of compression factor fluctuations.

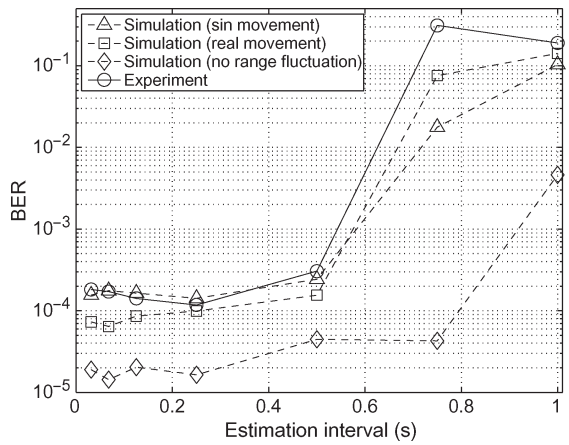

Fig. 13. BER versus the Doppler and channel estimation interval T_{est}.

the floor BER level is lower than in the other cases. Fig. 14 shows the MSE of the soft demodulation output in the receiver. Comparing it with results in Fig. 13, it is shown that the MSE exhibits a behavior similar to the BER performance. Thus, taking into account the range fluctuations in the trajectory is useful for accurate prediction of the receiver performance. Simulation of the real movement is possible if data as shown in Fig. 12(a) are available. If not, the sinusoidal movement

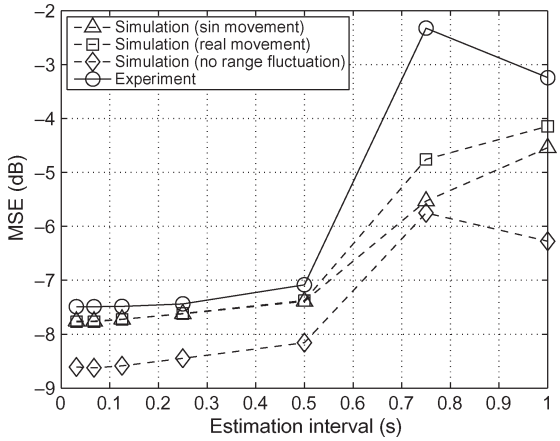

Fig. 14. MSE versus the Doppler and channel estimation interval T_{est}.

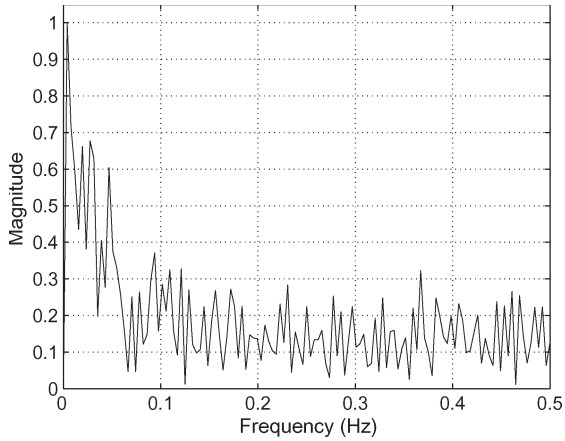

Fig. 15. Doppler spectrum of compression factor fluctuations obtained from the simulation: Scenario with no range fluctuation.

provides a good approximation to the scenario with the real movement.

V. Conclusion

In this paper, we have proposed a method for modeling underwater acoustic signal transmission for a moving transmitter and/or receiver, particularly for underwater acoustic communications. The proposed method is based on the approximation of the time-varying channel impulse response along the transmitter/receiver trajectory. This approach is implemented by sampling the trajectory and using local splines for the approximation. The proposed method has low complexity and low memory consumption. In addition, it can be implemented in a recursive form and, thus, can be used to develop real-time simulators for long-duration communication sessions. The proposed method has been verified by comparing the simulated data with data from real ocean experiments in shallow and deep water. For the shallow-water experiment, we have shown that the Doppler spectrum of the tones that were transmitted by a moving source is similar in the simulation and experiment. For the deep-water experiment, we have investigated the influence of the channel estimation interval on the detection performance of an OFDM receiver. It has been shown that the receiver performance is similar in the simulation and experiment.

However, note that the two experiments used to verify the channel model exploited low-frequency signals: 49–388 Hz in the shallow water and 2560–3584 Hz in the deep water. Therefore, the verification using experiments with signal transmission at higher frequencies is highly desirable. In addition, in the experiments used for the verification, scattering from the sea surface was not essential for the acoustic propagation. However, in several practical situations, the surface has a significant impact on the propagated signal. Thus, the proposed method can be used to model the transmission of low-frequency acoustic signals for underwater communications and other systems where the source and/or receiver moves and in channels where the surface scattering is not significant. Verifying the channel model using higher frequency sea experiments and incorporating into the model effects of acoustic scattering from the sea surface are the subjects of our future research.

ACKNOWLEDGMENT

The authors would like to thank the anonymous reviewers for their valuable comments, which have helped to improve this paper.

REFERENCES

[1] J. Preisig, "Acoustic propagation considerations for underwater acoustic communications network development," *ACM SIGMOBILE Mobile Comput. Commun. Rev.*, vol. 11, no. 4, pp. 2–10, Oct. 2007.

[2] M. Stojanovic and J. Preisig, "Underwater acoustic communication channels: Propagation models and statistical characterization," *IEEE Commun. Mag.*, vol. 47, no. 1, pp. 84–89, Jan. 2009.

[3] I. F. Akyildiz, D. Pompili, and T. Melodia, "Underwater acoustic sensor networks: Research challenges," *Ad Hoc Netw.*, vol. 3, no. 3, pp. 257–279, May 2005.

[4] G. Bertolotto, T. Jenserud, and P. A. van Walree, "Initial design of an acoustic communication channel simulator," in *Proc. UDT Eur.*, Naples, Italy, Jun. 2007.

[5] C. Bjerrum-Niese and R. Lutzen, "Stochastic simulation of acoustic communication in turbulent shallow water," *IEEE J. Ocean. Eng.*, vol. 25, no. 4, pp. 523–532, Oct. 2000.

[6] T. H. Eggen, A. B. Baggeroer, and J. C. Preisig, "Communication over Doppler spread channels—Part I: Channel and receiver presentation," *IEEE J. Ocean. Eng.*, vol. 25, no. 1, pp. 62–71, Jan. 2000.

[7] M. Patzold, U. Killat, F. Laue, and Y. Li, "On the statistical properties of deterministic simulation models for mobile fading channels," *IEEE Trans. Veh. Technol.*, vol. 47, no. 1, pp. 254–269, Feb. 1998.

[8] Y. R. Zheng and C. Xiao, "Simulation models with correct statistical properties for Rayleigh fading channels," *IEEE Trans. Commun.*, vol. 51, no. 6, pp. 920–928, Jun. 2003.

[9] C. Xiao, Y. R. Zheng, and N. C. Beaulieu, "Novel sum-of-sinusoids simulation models for Rayleigh and Rician fading channels," *IEEE Trans. Wireless Commun.*, vol. 5, no. 12, pp. 3667–3679, Dec. 2006.

[10] X. Geng and A. Zielinski, "An eigenpath underwater acoustic communication channel model," in *Proc. IEEE OCEANS*, San Diego, CA, 1995, vol. 2, pp. 1188–1196.

[11] G. L. Stüber, *Principles of Mobile Communication*. Dordrecht, The Netherlands: Springer-Verlag, 2001.

[12] B. S. Sharif, J. Neasham, O. R. Hinton, and A. E. Adams, "A computationally efficient Doppler compensation system for underwater acoustic communications," *IEEE J. Ocean. Eng.*, vol. 25, no. 1, pp. 52–61, Jan. 2000.

[13] B. Li, S. Zhou, M. Stojanovic, L. Freitag, and P. Willett, "Multicarrier communication over underwater acoustic channels with nonuniform Doppler shifts," *IEEE J. Ocean. Eng.*, vol. 33, no. 2, pp. 198–209, Apr. 2008.

[14] S. Mason, C. Berger, S. Zhou, and P. Willett, "Detection, synchronization, and Doppler scale estimation with multicarrier waveforms in underwater acoustic communication," *IEEE J. Sel. Areas Commun.*, vol. 26, no. 9, pp. 1638–1649, Dec. 2008.

[15] C. R. Berger, S. Zhou, J. C. Preisig, and P. Willett, "Sparse channel estimation for multicarrier underwater acoustic communication: From subspace methods to compressed sensing," *IEEE Trans. Signal Process.*, vol. 58, no. 3, pp. 1708–1721, Mar. 2010.

[16] S. M. Flatte, "Wave propagation through random media: Contributions from ocean acoustics," *Proc. IEEE*, vol. 71, no. 11, pp. 1267–1294, Nov. 1983.

[17] C. Bjerrum-Niese, L. Bjorno, M. A. Pinto, and B. Quellec, "A simulation tool for high-data-rate acoustic communication in a shallow-water time-varying channel," *IEEE J. Ocean. Eng.*, vol. 21, no. 2, pp. 143–149, Apr. 1996.

[18] M. Siderius and M. B. Porter, "Modeling broadband ocean acoustic transmissions with time-varying sea surfaces," *J. Acoust. Soc. Amer.*, vol. 124, no. 1, pp. 137–150, Jul. 2008.

[19] D. B. Kilfoyle and A. B. Baggeroer, "The state of the art in underwater acoustic telemetry," *IEEE J. Ocean. Eng.*, vol. 25, no. 1, pp. 4–27, Jan. 2000.

[20] M. B. Porter, *The KRAKEN normal mode program (Draft)*. Washington, DC: Naval Res. Lab., 1992.

[21] M. B. Porter and H. P. Bucker, "Gaussian beam tracing for computing ocean acoustic fields," *J. Acoust. Soc. Amer.*, vol. 82, no. 4, pp. 1349–1359, Oct. 1987.

[22] A. Essebbar, G. Loubet, and F. Vial, "Underwater acoustic channel simulations for communication," in *Proc. IEEE OCEANS*, Brest, France, 1994, vol. 3, pp. 495–500.

[23] S. Yerramalli and U. Mitra, "On optimal resampling for OFDM signaling in doubly selective underwater acoustic channels," in *Proc. OCEANS*, 2008, pp. 1–6.

[24] Y. V. Zakharov and V. P. Kodanev, "Multipath Doppler diversity of OFDM signals in an underwater acoustic channel," in *Proc. IEEE Int. Conf. Acoust. Speech Signal Process.*, 2000, vol. 5, pp. 2941–2944.

[25] L. Yu and L. B. White, "Optimum receiver design for broadband Doppler compensation in multipath/Doppler channels with rational orthogonal wavelet signaling," *IEEE Trans. Signal Process.*, vol. 55, no. 8, pp. 4091–4103, Aug. 2007.

[26] Y. V. Zakharov and V. P. Kodanev, "Doppler scattering adapted reception in a hydroacoustic communication channel," *Acoust. Phys.*, vol. 41, no. 2, pp. 219–223, Mar. 1995.

[27] G. W. Wornell, "A Karhunen–Loeve-like expansion for 1/f processes via wavelets," *IEEE Trans. Inf. Theory*, vol. 36, no. 4, pp. 859–861, Jul. 1990.

[28] M. Visintin, "Karhunen–Loeve expansion of a fast Rayleigh fading process," *Electron. Lett.*, vol. 32, no. 18, pp. 1712–1713, Aug. 1996.

[29] Z. Tang and G. Leus, "Time-multiplexed training for time-selective channels," *IEEE Signal Process. Lett.*, vol. 14, no. 9, pp. 585–588, Sep. 2007.

[30] T. Zemen and C. F. Mecklenbrauker, "Time-variant channel estimation using discrete prolate spheroidal sequences," *IEEE Trans. Signal Process.*, vol. 53, no. 9, pp. 3597–3607, Sep. 2005.

[31] M. K. Tsatsanis and G. B. Giannakis, "Modeling and equalization of rapidly fading channels," *Int. J. Adapt. Control Signal Process.*, vol. 10, no. 2/3, pp. 159–176, Mar. 1996.

[32] F. Qu and L. Yang, "Basis expansion model for underwater acoustic channels?" in *Proc. MTS/IEEE OCEANS Conf.*, Quèbec City, QC, Canada, Sep. 2008, pp. 1–7.

[33] Y. V. Zakharov, T. C. Tozer, and J. F. Adlard, "Polynomial spline approximation of Clarke's model," *IEEE Trans. Signal Process.*, vol. 52, no. 5, pp. 1198–1208, May 2004.

[34] H. Mai, Y. V. Zakharov, and A. G. Burr, "Iterative channel estimation based on B-splines for fast flat-fading channels," *IEEE Trans. Wireless Commun.*, vol. 6, no. 4, pp. 1224–1229, Apr. 2007.

[35] N. P. Korneichuk, *Exact Constants in Approximation Theory*. Cambridge, U.K.: Cambridge Univ. Press, 1991.

[36] V. M. Tikhomirov, "Harmonics and splines as optimal tools for approximation and recovery," *Russian Math. Surveys*, vol. 50, no. 2, pp. 355–402, 1995.

[37] M. Unser, A. Aldroubi, and M. Eden, "B-spline signal processing—Part I: Theory," *IEEE Trans. Signal Process.*, vol. 41, no. 2, pp. 821–833, Feb. 1993.

[38] V. A. Zheludev, "Asymptotic formulae for local spline approximation on a uniform grid," *Doclady Academii Nauk*, vol. 269, no. 4, pp. 797–802, 1983.

[39] V. A. Zheludev, "Local spline approximation on a uniform grid," *Comput. Maths Math. Phys.*, vol. 27, no. 9, pp. 1296–1310, 1987.

[40] Y. V. Zakharov and T. C. Tozer, "Frequency estimator with dichotomous search of periodogram peak," *Electron. Lett.*, vol. 35, no. 19, pp. 1608–1609, Sep. 1999.

[41] S. D. Chuprov, "Interference structure of an acoustic field in a layered waveguide," in *Proc. Ocean Acoust.*, L. M. Brekhovskikh and I. B. Andreevoi, Eds., Moscow, Russia, 1982, pp. 71–91.
[42] G. A. Grachev, "Theory of acoustic field invariants in layered waveguides," *Acoust. Phys.*, vol. 39, no. 1, pp. 33–35, Jan. 1993.
[43] M. Porter, *Bellhop Gaussian Beam/Finite Element Beam Code*. Available in the Acoustics Toolbox. [Online]. Available: http://oalib.hlsresearch.com/Rays
[44] J. Murray and D. Ensberg, *The SWellEx-96 Experiment*. [Online]. Available: http://www.mpl.ucsd.edu/swellex96/
[45] T. Chen, C. Liu, and Y. V. Zakharov, "Matched-phase coherent broadband matched-field processor using phase descent search," in *Proc. 10th ECUA*, 2010, pp. 590–595.
[46] C. Liu, T. Chen, and Y. V. Zakharov, "Source localization using sparsity-based iterative adaptive beamforming," in *Proc. 10th ECUA*, 2010, pp. 604–610.
[47] Z. Xu, Y. V. Zakharov, and V. P. Kodanev, "Space–Time signal processing of OFDM signals in fast-varying underwater acoustic channel," in *Proc. OCEANS*, Aberdeen, U.K., 2007, pp. 1–6.
[48] J. G. Proakis, *Digital Communications*. New York: McGraw-Hill, 1995.
[49] Y. V. Zakharov, V. M. Baronkin, and T. C. Tozer, "DFT-based frequency estimators with narrow acquisition range," *Proc. Inst. Elect. Eng. Commun.*, vol. 148, no. 1, pp. 1–7, Feb. 2001.
[50] R. H. Owen, B. V. Smith, and R. F. W. Coates, "An experimental study of rough surface scattering and its effects on communication coherence," in *Proc. OCEANS*, Brest, France, 1994, vol. 3, pp. 483–488.
[51] Y. V. Zakharov and V. P. Kodanev, "Noise immunity of adaptive reception of complex acoustic signals in the presence of reflections from ocean boundaries," *Acoust. Phys.*, vol. 42, no. 2, pp. 185–191, Mar. 1996.
[52] M. Badiey, Y. Mu, J. A. Simmen, and S. E. Forsythe, "Signal variability in shallow-water sound channels," *IEEE J. Ocean. Eng.*, vol. 25, no. 4, pp. 492–500, Oct. 2000.

Chunshan Liu received the B.S. degree in physics in 2007 from the University of Science and Technology of China, Hefei, China, and the M.Sc. (with distinction) degree in communication engineering in 2008 from the University of York, York, U.K., where he is currently working toward the Ph.D. degree in communication engineering with the Department of Electronics.

His research interests include adaptive array processing for underwater acoustics, signal processing for communications, and compressed sensing.

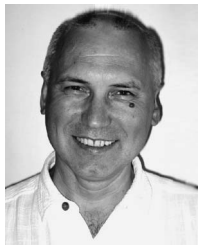

Yuriy V. Zakharov (M'01–SM'12) received the M.Sc. and Ph.D. degrees in electrical engineering from Moscow Power Engineering Institute, Moscow, Russia, in 1977 and 1983, respectively.

From 1977 to 1983, he was an Engineer with the Special Design Agency, Moscow Power Engineering Institute. From 1983 to 1999, he was the Head of Laboratory with the N. N. Andreev Acoustics Institute, Moscow. From 1994 to 1999, he was with Nortel as a DSP Group Leader. Since 1999, he has been with the Communications Research Group, University of York, York, U.K., where he is currently a Reader with the Department of Electronics. His research interests include signal processing and communications.

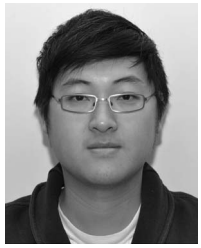

Teyan Chen received the B.Sc. degree from the University of Central Lancashire, Preston, U.K., in 2005 and the M.Sc. and Ph.D. degrees in electronic engineering from the University of York, York, U.K., in 2006 and 2011, respectively.

He is currently with the Department of Electronics, University of York. His research interests include adaptive filtering, equalization, wireless communications, and underwater acoustic communications.